

SonoTweezer: An Acoustically Powered End-Effector for Underwater Micromanipulation

Sumit Mohanty¹, Robbert-Jan Fidler¹, Pedro M. Matos, Christoff M. Heunis², *Student Member, IEEE*, Mert Kaya³, *Student Member, IEEE*, Nathan Blanken¹, and Sarthak Misra⁴, *Senior Member, IEEE*

Abstract—Recent advances in contactless micromanipulation strategies have revolutionized prospects of robotic manipulators as next-generation tools for minimally invasive surgeries. In particular, acoustically powered phased arrays offer dexterous means of manipulation both in air and water. Inspired by these phased arrays, we present SonoTweezer: a compact, low-power, and lightweight array of immersible ultrasonic transducers capable of trapping and manipulation of sub-mm sized agents underwater. Based on a parametric investigation with numerical pressure field simulations, we design and create a six-transducer configuration, which is small compared to other reported multi-transducer arrays (16–256 elements). Despite the small size of array, SonoTweezer can reach pressure magnitudes of 300 kPa at a low supply voltage of 25 V to the transducers, which is in the same order of absolute pressure as multi-transducer arrays. Subsequently, we exploit the compactness of our array as an end-effector tool for a robotic manipulator to demonstrate long-range actuation of sub-millimeter agents over a hundred times the agent's body length. Furthermore, a phase-modulation over its individual transducers allows our array to locally maneuver its target agents at sub-mm steps. The ability to manipulate agents underwater makes SonoTweezer suitable for clinical applications considering water's similarity to biological media, e.g., vitreous humor and blood plasma. Finally, we show trapping and manipulation of micro-agents under medical ultrasound (US) imaging modality. This application of our

actuation strategy combines the usage of US waves for both imaging and micromanipulation.

Index Terms—Acoustic levitation, haptics, medical robotics, microrobots, phased arrays, robotic manipulator, ultrasonics, ultrasound (US) imaging, waterborne.

I. INTRODUCTION

IN RECENT years, diverse clinical applications have advanced owing to the dexterity and precision of contactless micromanipulation methods that encompass robotics and microsystem technology [1]. Furthermore, the clinical compatibility with magnetic resonance (MR) and ultrasound (US) imaging have favored the outreach of magnetic and acoustic methods for remote manipulation [2], [3]. With the ability to manipulate agents across different length scales, acoustically powered devices facilitate the most diverse applications, from lab-on-a-chip diagnostics, to minimally invasive surgeries [4]. These devices, commonly known as acoustic tweezers, consist of multiple piezoelectric transducers that generate pressure fields to trap and manipulate agents [5]. The ability to generate and steer such pressure fields enables these tweezers to perform sophisticated interventions such as medical expulsive therapy, in a minimally invasive manner [6].

Among acoustic tweezers, many ultrasonic phased arrays have been reported for mid-air levitation of millimeter-sized agents [7]–[11]. These arrays exist in various morphologies of transducers and phase distribution across transducers, which enable spatio-temporal modulation of pressure fields around them [9]. Moreover, the inexpensive, modular, and accessible hardware components in such arrays have paved the way for many open-source research systems [9]–[11]. Despite the ubiquity of the phased arrays, the majority of them are airborne systems. Previously, the acoustic tweezers for waterborne applications have been either limited to 2-D microchannels [12] or enclosed volumes inside bulk resonant chambers [13]. In the case of microchannels, the tweezers are confined to surface manipulation of micro-agents [4]. Contrarily, acoustic resonant chambers operate only on bounded fluid reservoirs with limited arrangement patterns of target agents.

As most *in vivo* clinical applications require instrumentation that is compatible with biological media like blood plasma and vitreous humor, a new kind of waterborne tweezers have emerged as a potential solution [6], [14]–[18]. The phased arrays for airborne applications described earlier are realized with immersible high-frequency transducers that generate

Manuscript received November 17, 2021; accepted January 3, 2022. Date of publication January 6, 2022; date of current version March 3, 2022. This work was supported by the Netherlands Organization for Scientific Research (Innovational Research Incentives Scheme–VIDI: SAMURAI Project # 14855). (Corresponding author: Sumit Mohanty.)

Sumit Mohanty, Robbert-Jan Fidler, and Christoff M. Heunis are with the Surgical Robotics Laboratory, Department of Biomechanical Engineering, University of Twente, 7500 AE Enschede, The Netherlands (e-mail: s.mohanty@utwente.nl; r.fidler@student.utwente.nl; c.m.heunis@utwente.nl).

Pedro M. Matos is with the Surgical Robotics Laboratory, Department of Biomechanical Engineering, University of Twente, 7500 AE Enschede, The Netherlands, and also with the Faculdade de Engenharia da Universidade do Porto, 4200-465 Porto, Portugal (e-mail: p.mendesantunesdematos@student.utwente.nl).

Mert Kaya and Sarthak Misra are with the Surgical Robotics Laboratory, Department of Biomechanical Engineering, University of Twente, 7500 AE Enschede, The Netherlands, and also with the Department of Biomedical Engineering, University of Groningen and University Medical Center Groningen, 9713 AV Groningen, The Netherlands (e-mail: kaya@utwente.nl; m.kaya@umcg.nl; s.misra@utwente.nl; s.misra@umcg.nl).

Nathan Blanken is with the Physics of Fluids Group, MESA+ Institute for Nanotechnology, Technical Medical (TechMed) Centre, University of Twente, 7500 AE Enschede, The Netherlands (e-mail: n.blanken@utwente.nl).

This article has supplementary downloadable material available at <https://doi.org/10.1109/TUFFC.2022.3140745>, provided by the authors.

Digital Object Identifier 10.1109/TUFFC.2022.3140745

steerable acoustic beams to trap and maneuver agents in an open workspace underwater. As a result, these immersible phased arrays can manipulate sub-mm to micro-scale agents in deep-seated tissues of the body thereby, making clinical operations less invasive [6], [15], [18].

However, the integration of these immersible arrays into clinical systems is limited for a couple of reasons. First, these arrays often require a large number of sophisticated transducers that are high-end commercial products such as systems developed by Verasonics Inc., Kirkland, WA, USA [6], Imasonic SAS, Voray-sur-l'Ognon, France, [15], and Phillips B.V., Eindhoven, The Netherlands [17]. Furthermore, the overall cost in such a system integration is also burdened by the expensive peripheral equipment employed for functions such as pressure amplification and data acquisition. Moreover, the large number of transducers adds to the overall size and weight of such a system. Hence, it becomes difficult to interface such large transducer arrays with other automated equipment, such as robotic manipulators, that could be useful for clinical applications [19], [20]. Besides, various clinical applications require the usage of micro-agents to perform operations such as targeted therapy and drug delivery [1]. For such clinical applications, the large size of such transducer arrays makes it challenging to reliably locate sub-mm agents in their target workspace that spans a few centimeters [21].

Contactless manipulators are not only used as standalone devices, but also as auxiliary tools to minimize interventions during clinical operations [22]–[28]. Notably, robotic manipulators with magnetic end-effectors can perform clinical operations such as catheterization under *ex-vivo* conditions [23]. However, such robotic systems mostly utilize bulky permanent magnets or electromagnets that restrict the payload carrying capacity of the manipulator [24], [25]. Furthermore, the high magnetic fields generated by these systems (up to 200 mT) may interfere with auxiliary electronic components employed during the clinical operation [26]. Alternatively, ultrasonic phased arrays are lightweight and possess noninterfering hardware. Thus, these phased arrays can be a safer substitute for magnetic coils as an end-effector for robotic manipulation. Recently, airborne phased arrays mounted on a robotic manipulator have demonstrated pick-and-place of millimeter-sized agents over long distances [27], [28]. This provides an opportunity to redesign immersible phased arrays as end-effectors suitable for micromanipulation in biological media.

In this article, we present SonoTweezer, a compact and lightweight acoustic tweezer that addresses the limitations of the aforementioned phased arrays and is compatible with integration into robotic systems. SonoTweezer is an array of six immersible waterborne transducers in a close-packed spatial configuration that can trap milli- to micro-sized agents at their focal point (see Fig. 1). With this compact design, we achieve comparable pressure magnitudes for manipulation with lower power requirements in contrast to other waterborne arrays.

We first investigate various design metrics of SonoTweezer based on numerical computations and validate the resultant pressure fields with hydrophone measurements. Second, we demonstrate trapping and localized manipulation of

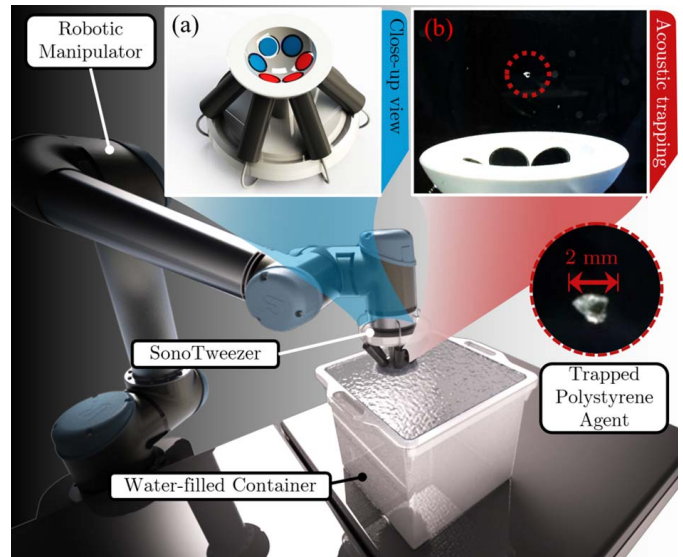


Fig. 1. Schematic depicts a robotic manipulator carrying SonoTweezer as an end-effector for manipulation of agents immersed in a water-filled container. (a) Close-up of SonoTweezer with the transducer heads labeled with color schemes (red for 0° and blue for 180°) that describe the phase of the emitted wave, and (b) shows a 2-mm Polystyrene agent trapped at SonoTweezer’s focal point.

micro-agents (size $\sim L$) with manually controlled motion of SonoTweezer under both optical and US imaging. Finally, we mount SonoTweezer to a robotic manipulator (UR5, Universal Robots, Odense, Denmark) and demonstrate long-distance ($\sim 100L$) manipulation of the agent underwater. Thus, the compactness of SonoTweezer enables a robotic manipulator to move micro-agents in liquids across distances of up to two orders higher than their body length in a contactless manner.

II. MATERIALS AND METHODS

In this section, we discuss the design, trapping strategy, modeling, and experimental validation of SonoTweezer. First, we present the theory of radiation forces followed by simulation of acoustic pressure fields generated by a hemispherical array of transducers. Next, we measure the pressure generated by our chosen immersible transducer for an estimate of its maximum pressure and its focal point. Then, we compute the acoustic fields and the resultant forces on a target micro-agent with our model and evaluate various design parameters for the construction of our array. In addition, we validate our computational model by reproducing the acoustic field generated by Ultraino [29]. Finally, we experimentally characterize SonoTweezer and measure the overall pressure distribution around the array to compare the pressure magnitudes achieved with the simulations.

A. Modeling of Acoustic Forces

The propagation of sound waves through a liquid subjects the agents immersed in it to acoustic radiation forces [4]. For agents (size $\sim L$) that are significantly smaller than the acoustic wavelength (λ) i.e., $\lambda \gg L$, radiation forces ($\mathbf{F}_{\text{rad}} \in \mathbb{R}^3$) acting on them can be written as gradient forces.

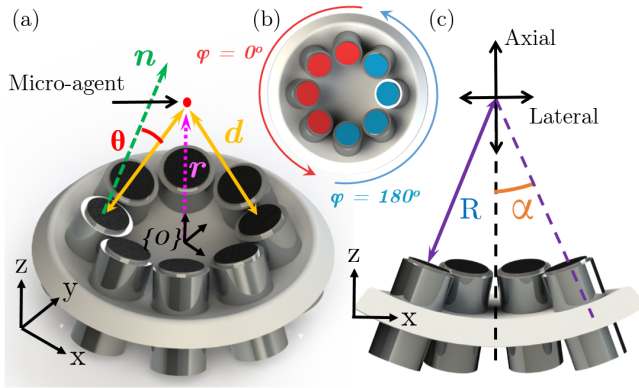


Fig. 2. (a) Transducer and array geometry: Euclidian distance (d) and angle (θ) of each transducer with respect to the micro-agent. The agent is at a distance (r) with respect to the Origin $\{O\}$, situated at the center of the array, and at a distance d_i from every i -th transducer. θ_i is the angle between the outward normal vector, (n_i) from the piston's surface and vector along d_i from each transducer. (b) Phase at which every i -th transducer emits is φ_i . Here, the phase distribution of the array is in twin trap configuration with half of the transducers in anti-phase to the other. (c) Transducer array parameters: R denotes the radius of the hemispherical array and α is the angle between the central axis and the circular ring of transducers. The transducers are aligned in such a way that the geometrical focal point of the cap aligns with the desired trapping position, referred to as focal trap.

The radiation force on a small, spherical particle of radius (r_p) can be expressed as

$$\mathbf{F}_{\text{rad}} = -\nabla U \quad (1)$$

where U is known as the Gor'kov potential [30]. Assuming a low-amplitude, sinusoidal pressure variation in an inviscid medium, U can be expressed as

$$U = 2\nu(\|P\|^2) - 2\xi\left(\left\|\frac{\partial P}{\partial x}\right\|^2 + \left\|\frac{\partial P}{\partial y}\right\|^2 + \left\|\frac{\partial P}{\partial z}\right\|^2\right) \quad (2)$$

where P is the complex acoustic pressure amplitude at a point in the field, and the $\|$ denotes its absolute value. Also, ν and ξ are constants that describe the acoustic contrast of particle relative to the medium such that

$$\begin{aligned} \nu &= \frac{\pi r_p^3}{6c_0^2\rho_0}K_1 = \frac{\pi r_p^3}{6}\left(\frac{1}{c_0^2\rho_0} - \frac{1}{c_p^2\rho_p}\right) \\ \xi &= \frac{r_p^3}{16\pi f_0^2\rho_0}K_2 = \frac{r_p^3}{8\pi f_0^2}\left(\frac{\rho_p - \rho_0}{\rho_0(\rho_0 + 2\rho_p)}\right) \end{aligned} \quad (3)$$

where r_p is the particle radius, f is the frequency of sound, c is the speed of sound, and ρ is the density (the subscripts p and 0 denote the particle and medium, respectively). Here, K_1 and K_2 describe the relative acoustic contrast [30] such that, $K_1 = 0.6$ and $K_2 = 0.03$ calculated with the properties of the medium and the particle (see Table I). A derivation of (2) from the original form of Gor'kov potential is described in supplementary information (SI) Appendix A.

Next, we approximate the acoustic pressure generated by our immiscible transducers with a flat piston source model [31]. Given the number of transducers (N_t) in a hemispherical array, assigned with a normalized pressure constant (p_0), the overall pressure field can be computed based on the superposition principle [11]. Here, the normalized pressure

TABLE I
INITIAL PARAMETERS FOR THE TRANSDUCER ARRAY

Variable	Ultratino	SonoTweezer	Units	Definition
c_0	343	1510	m/s	Speed of sound in medium (25°C)
ρ_0	1.18	997	kg/m ³	Density of medium
c_p	900	2350	m/s	Speed of sound in agent (25°C)
ρ_p	29	1050	kg/m ³	Density of agent
r_p	500	250	μm	Radius of spherical agent
N_t	44	6	–	Number of transducers
R	61	20	mm	Radius of hemispherical array cap
α	15	30	°	Transducer angle (Fig. 2c)
f	41	1000	kHz	Center frequency of transducer
a	4.5	6.5	mm	Radius of transducer
p_0	0.17	73	Pa·m/V	Normalized Pressure constant (4)

constant, p_0 , is the transducer amplitude (in Pa) normalized to the distance of measurement location from transducer (d) and the applied supply voltage (V), described later in Section II-C1. For each i -th transducer, the pressure response at any point ($\mathbf{r} = [x \ y \ z]^T \in \mathbb{R}^3$) with respect to the origin of the frame ($\{O\}$) depends on its propagation distance from the transducer (d_i), its angle of orientation, (θ_i), and corresponding phase delay, (φ_i). These geometrical parameters are calculated with respect to the transducer normal, ($\mathbf{n} \in \mathbb{R}^3$) as shown in Fig. 2(a). Based on far-field approximation (i.e., $d \gg a^2/\lambda^2$) and paraxial approximation (i.e., $\sin\theta \approx \theta$), the acoustic pressure at point ($\mathbf{r} \in \mathbb{R}^3$) as a result of superposition from (N_t) transducers can be expressed as

$$P(\mathbf{r}) = \sum_{i=1}^{N_t} \frac{p_0 V}{d_i} \left\{ \frac{2J_1(ka \sin\theta_i)}{ka \sin\theta_i} \right\} e^{j(\varphi_i - kd_i)} \quad (4)$$

where J_1 is a first order Bessel function of the first kind, a is the transducer radius, $k = 2\pi/\lambda$ is the wavenumber, and λ is the wavelength [11]. Furthermore, the phase distribution of the transducers (φ) determines the manipulation strategy to trap the micro-agents. The most commonly used strategies in phased arrays are referred to as twin trap and vortex trap. Although vortex traps are more commonly employed, they could result in rotational instabilities of the target agent which might eject the agent out of its trapped location [32]. Hence, we choose the twin trap strategy, which uses a convenient binary distribution, i.e., $\varphi = 0^\circ$ or 180° [see Fig. 2(b)]. Finally, we compute the acoustic pressure and the resultant radiation forces on a target agent and evaluate the design parameters of the array as described in Fig. 2(c).

B. Computation of Acoustic Forces

Based on (1)–(4), we developed a computational model to generate 3-D acoustic pressure fields for our transducer array using MATLAB (R2021a, Mathworks Inc., Natick, MA, USA). We simulate the pressure field and corresponding radiation forces on a target agent based on certain initial array parameters and physical properties of the agent and medium (see Table I). We describe the measured value of $p_0 = 73$ Pa·m/V used in the simulations as described in Section II-C1. Here, we first choose an initial trapping position

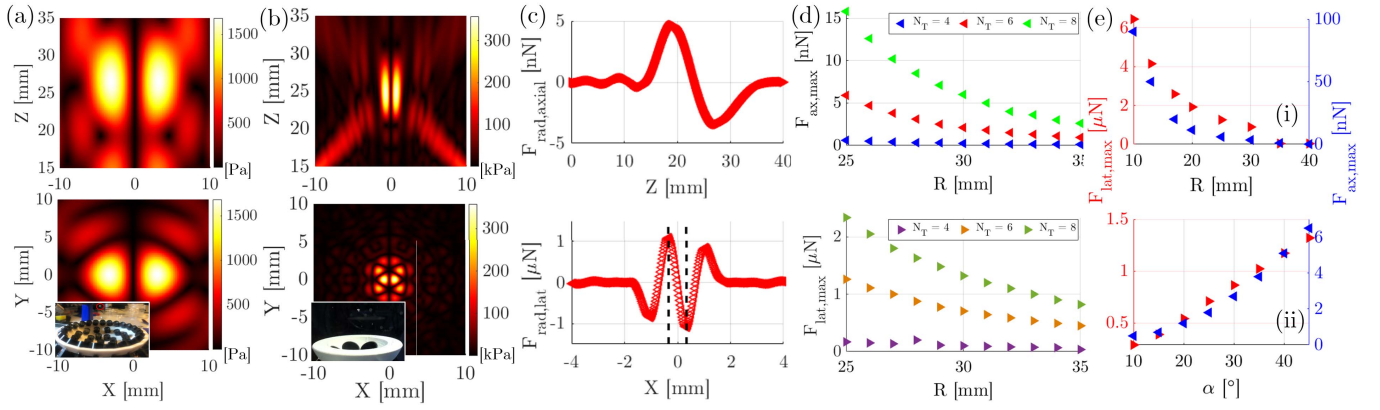


Fig. 3. Numerical computation of acoustic pressure fields of twin trap based arrays: (a) Ultraino [29]: Pressure field map generated by the transducer array ($R = 61$ mm, $\alpha = 15^\circ$, $N_t = 44$ distributed over three rings {8, 12, 24}) at 40 kHz in XY and XZ planes, respectively. (b) SonoTweezer: Pressure field map generated by the transducer array ($R = 27$ mm, $\alpha = 43^\circ$, $N_t = 6$) at 1 MHz in XY and XZ planes, respectively. Inset in (a) and (b) show the respective transducer arrays. (c) Radiation forces acting on a 0.5-mm Polystyrene agent represented as $F_{\text{rad,axial}}$ and $F_{\text{rad,lat}}$ in X -(lateral) and Z -(axial) directions, respectively. The black dotted lines represent the trapping region between the two pressure maxima shown as pressure lobes in (b). (d) and (e) Parametric evaluation of maximum $|F_{\text{rad,axial}}|$ and $|F_{\text{rad,lat}}|$ for varying array parameters: (d) Trapping forces as a function of R , for different N_t . (e) For a fixed $N_t = 6$, evaluation of maximum $|F_{\text{rad,axial}}|$ and $|F_{\text{rad,lat}}|$ for changing (i) R , and (ii) α .

of the array ($\mathbf{r} \in \mathbb{R}^3$) and define a 3-D grid of 800 points each in X, Y, Z around this position. Second, we define the transducer parameters for our array (d_i, θ_i, ϕ_i) with respect to every point (\mathbf{r}). Next, we calculate the resultant pressure field over this grid using (4). Similar to arrays like Ultraino [11], we show the pressure fields in two orthogonal 2-D slices namely, XY and XZ planes, respectively centered around $z = R_i$ [see Fig. 2(c)]. In these planes, we compute the radiation forces on a target agent in lateral and axial directions with respect to the array, represented as $F_{\text{rad,lat}}$ and $F_{\text{rad,axial}}$, respectively. Fig. 3 summarizes the key results of our computational study.

1) *Simulation of SonoTweezer Fields:* First, we simulate the acoustic pressure field of Ultraino array in order to validate our simulation model. Fig. 3(a) represents the simulated acoustic pressure field in the XY and XZ planes centered at the focal point of the array along the Z -axis ($Z = R$). These central-axial pressure maps of our array coincide with those reported in [11]. Importantly, we find a double-lobed pressure maximum in both the planes separated by a pressure minimum which is characteristic of the trapping region in a twin trap. This replication study provides us with a ground truth to validate our computational model using an existing array design with comparable pressure magnitudes. Next, we simulate our waterborne transducer array with the respective variables (see Table I) to locate its trapping region [see Fig. 3(b)]. Similar to Ultraino, the pressure lobes of our array give rise to a large potential field based on (2) and thus, large radiation forces ($F_{\text{rad}} \in \mathbb{R}^3$) that converge at the trap. We decompose and quantify these forces as axial and lateral components namely, $F_{\text{rad,axial}}$ along the Z -direction, and $F_{\text{rad,lat}}$ along the X -direction [see Fig. 3(c)]. Moreover, as $F_{\text{rad,axial}}$ are the weakest, and $F_{\text{rad,lat}}$ are the dominant features of a twin trap [16], we use their respective maximum values of both to evaluate various design parameters (R, α, N_t) of our array [see Fig. 3(b)]. For comparison with [11], we compute the maximum value of these forces that Ultraino exerts on an expanded

polystyrene particle ($d_p = 1$ mm) as $F_{\text{rad,axial}} = 350$ nN and $F_{\text{rad,lat}} = 2$ μ N. For SonoTweezer, we calculate the trapping forces on a polystyrene agent ($d_p = 0.5$ mm) as $F_{\text{rad,axial}} = 5$ nN and $F_{\text{rad,lat}} = 1$ μ N. Besides the double-lobed pressure profile, we also encounter other sidelobes around the trapping region [see Fig. 3(b)]. We evaluate the trapping forces at these positions to be $F_{\text{rad,axial}} = 20$ nN and $F_{\text{rad,lat}} = 0.5$ μ N, respectively (see SI Appendix B). The higher values of $F_{\text{rad,axial}}$ at these sidelobes are due to the inclined nature of these lobes whereby a lateral pressure component also contributes to the overall force in the axial direction. Nevertheless, the higher magnitude of dominant $F_{\text{rad,lat}}$ at the double-lobed trap that at the sidelobes suggests a higher probability of trapping at the central pressure minima in the double-lobed profile. Last, while a few micro-agents are occasionally trapped in these sidelobes, we find that they are ejected as soon as SonoTweezer is moved. Thus, only the agents trapped between the double-lobed profile retain their position during our subsequent experiments.

2) *Optimization of Array Parameters:* We start our investigation with the minimum number of transducers (N_t) required to construct our array [see Fig. 3(d)]. Here, we vary the cap radius (R) and transducer angle (α), in chosen combinations that the array geometry allows, to evaluate the forces ($F_{\text{rad,axial}}, F_{\text{rad,lat}}$). We find that increase in N_t leads to increase in $F_{\text{rad,axial}}$ and $F_{\text{rad,lat}}$ for decreasing R (and increasing α). Although $N_t = 8$ gives the highest forces, $N_t = 4$ results in the smallest array size. However, the trapping forces in case of $N_t = 4$ are an order of magnitude lower than $N_t = 6$. Hence, we choose six transducers for our array since it provides us the smallest configuration without significant reduction in the forces, i.e., nearly the same order of magnitude as $N_t = 8$.

Next, we vary combinations of R and α for $N_t = 6$ to estimate the variation in these forces [see Fig. 3(e)]. First, we observe that an increase in R results in a decrease in both $F_{\text{rad,axial}}$ and $F_{\text{rad,lat}}$. However, the measured focal distance of our transducer is in the range of 20–30 mm [see Fig. 4(a)],

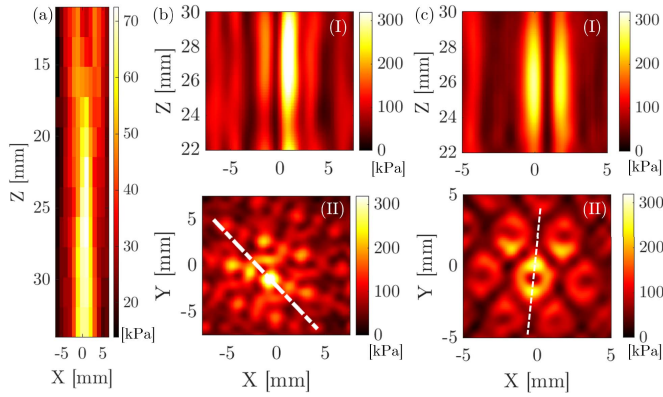


Fig. 4. Acoustic characterization of: (a) single transducer, (b) array of six transducers, i.e., SonoTweezer, and (c) SonoTweezer with phase compensation. (a) Central axial pressure profile of a single immersible transducer. Maximum pressure amplitude (~ 73 kPa) occurs at 28 mm from the center of the transducer [i.e., $(X = 0, Z = 0)$]. Interpolated lateral acoustic pressure profile in XY plane at the focal point of SonoTweezer, i.e., $R = 27$ mm: (b.II) without any phase compensation, and (c.II) after phase compensation. The white line in both (b.II) and (c.II) indicates the orientation of the axial plane shown in XZ plane. Interpolated axial profile of the transducer based on lateral scans performed between $Z = 22$ mm and $Z = 30$ mm: (b.I) without any phase compensation, and (c.I) after phase compensation. For (b) and (c), we drive our transducer(s) with a 1-MHz signal in burst mode (30 cycles) at $V = 25 V_{pp}$.

we prefer R to be within this range. Second, both $F_{rad,axial}$ and $F_{rad,lat}$ increase with α . For each case in Fig. 3(e)(i) and (ii), R and α are varied in specific combinations that are permitted by the array geometry. Thus, for $20 \text{ mm} \leq R \leq 30 \text{ mm}$, we have an allowed range of $35^\circ \leq \alpha \leq 45^\circ$. Overall, based on the aforementioned findings, we choose the final array parameters to be $R = 27$ mm and $\alpha = 43^\circ$.

Besides the acoustic forces, we also compute the net force imbalance on the agent to overcome the effects of gravity and buoyancy, i.e., $F_{net} = 34$ nN (see SI Appendix C). Although the theoretical computation suggests $F_{rad,axial} < F_{net}$, we are yet able to trap various micro-agents with $N_t = 6$ transducers (discussed in Section III-B). We explain these trapping experiments in contrast to theoretical predictions with the limited validity of the Gor'kov theory. This theory suggests that (2) is valid when agent size is significantly smaller than the acoustic wavelength. In our case, owing to comparable agent size to the acoustic wavelength for a 0.5-mm agent, i.e., $\lambda \sim L$, (2) does not accurately account for the radiation forces [33]. Nevertheless, we proceed with $N_t = 6$ as our design choice for SonoTweezer in subsequent experiments.

C. Characterization of Acoustic Pressure

In this section, we describe the acoustic pressure characterization of a single immersible transducer (1 MHz, Imasonic SAS), and that of the array comprising of six such transducers. We use a fiber-optic needle hydrophone (Precision-Acoustics, Dorchester, U.K.) mounted on a motorized stage to characterize the transducers based on their burst-mode operation. An elaborate description of the measurement setup and data processing can be found in SI Appendix D and E.

1) *Measured Pressure From a Single Transducer*: The theoretical value of focal distance for a given transducer where it generates maximum pressure (P_{max}) is given as [34]

$$R_{th} = \frac{(2 \cdot a)^2}{4\lambda} = 28 \text{ mm.} \quad (5)$$

Based on Fig. 4(a), P_{max} occurs in the range $22 \text{ mm} \leq Z \leq 27 \text{ mm}$. Hence, we choose $d_0 = R = 25$ mm as our desired focal point and we calculate the p_0 using (4) as

$$p_0 = \frac{P_{max} \cdot d_0}{V_0} = 73 \text{ Pa} \cdot \text{m/V} \quad (6)$$

where $V_0 = 25 V_{pp}$ is the driving voltage of the transducer.

2) *Scanned Acoustic Profile of SonoTweezer*: In case of SonoTweezer, we first scan the pressure field in the XY plane of the array for a range of values along the Z -axis centered around the focal point [see Fig. 4(b.II) and (c.II)]. Second, we reconstruct the axial pressure field in the XZ plane based on the interpolated values of pressure scans previously obtained in XY plane [see Fig. 4(b.I) and (c.I)]. Additional details on the pressure map interpolation is described in SI Appendix F, G, and H. We initially find that the measured pressure profile in the lateral plane has unequal magnitudes of the two central lobes which could make the trapping of agents less efficient [see Fig. 4(b.I)]. We attribute this imbalance between the pressure lobes to the undesired phase delays between the transducers. Similar observations have been previously reported with immersible tweezers at high frequency (> 1 MHz) caused by fabrication errors or imprecision in positioning of the transducers [16], [35]. We account for such undesired phase delays in our simulations by providing an additional phase offset ($\Delta\phi$) to the transducers. As described in SI Appendix G, such an offset compensates for the additional distance sound waves travel owing to the causes highlighted above.

Although we perform our trapping experiments with the initially observed pressure profile [see Fig. 4(b)], we later compensate for the imbalanced pressure response of SonoTweezer based on phase adjustments of the transducers. In order to compensate for these imbalanced pressure lobes, we measure the pressure map generated by each of the opposite pairs of transducers. Based on the measurements described in SI Appendix H, we estimate an additional phase offset of ($\Delta\phi = 144^\circ$), that compensates for the imbalanced pressure lobes observed earlier with our measurements [see Fig. 4(c)]. Nevertheless, we are able to achieve a trapping region between these lobes with pressure magnitudes of up to 250–300 kPa. In comparison to this value, previously reported waterborne tweezers reach pressure magnitudes in the range 750 kPa–1 MPa [6], [15], [16]. Hence, the close-packed distribution of transducers in SonoTweezer enables us to achieve similar order of pressure magnitudes with a low driving power, i.e., $25 V_{pp}$ as compared to other multi-transducer arrays.

D. Design and Assembly of SonoTweezer

SonoTweezer comprises six immersible US transducers (13-mm diameter, 01480XCR01, Imasonic SAS) assembled

in a 3-D printed frame made up of Acrylonitrile Butadiene Styrene (ABS) (see Fig. 1). It is powered with a waveform generator (33510B, Keysight Inc., Santa Rosa, CA, USA) that supplies a 1-MHz continuous sine wave which is amplified using a voltage amplifier (ESyLAB LM3325 eight-channel [36]) up to $25 V_{pp}$. Micro-agents for the experiments are synthesized by grinding polystyrene pellets (430102-1KG, Sigma-Aldrich, St. Louis, MO, USA) with dry ice (-78°C) in a blender (Mia GY-701, Freihafen, Duisburg, Germany) for 2 min. Polystyrene micro-agents in the 0.5–2-mm-size range are collected by evaporating dry ice at room temperature overnight [37]. Optical vision throughout the experiments is provided using two CMOS cameras (MC031CG-SY-UB and MQ013CG-ON, XIMEA, Münster, Germany) attached to their respective lenses [M0814-MP2 (COMPUTAR, USA) and LM12J5M2 (KOWA LENS, Nagoya, Aichi, Japan)]. All the video processing is done in MATLAB. Additionally, localized manipulation of micro-agents is performed under US imaging and acquisition system (L15 HD Scanner, Clarius Mobile Health, Vancouver, BC, Canada) with an imaging frequency of 14 MHz. For experiments with hand-held operation of SonoTweezer, the array is placed in a cubical acrylic box of side 100 mm. Finally, SonoTweezer is mounted on a robot manipulator [23] (UR5, Universal Robots) for the long-distance manipulation experiments in a storage box as workspace (570 mm \times 390 mm \times 280 mm, IKEA).

III. RESULTS AND DISCUSSION

We performed experiments in which we trap PS agents at the simulated trapping point of SonoTweezer and manipulate them across distances under manual movement of the array and when interfaced to a robotic end-effector. We first demonstrate trapping and motion of agents local to their focal point under phase-controlled manipulation (see Section III-A). Second, we study the stability of the acoustic trap for varying sizes of our agents (see Section III-B). Third, we demonstrate the motion of the trapped agents with handheld or manual movement of the array under both optical camera and US imaging (see Section III-C). Finally, we demonstrate motion of our trapped target agent under open-loop manipulation of the robotic manipulator's end-effector (see Section III-D). Full demonstrations of the aforementioned results are available in the Supplementary Movies (S1–S4).

A. Phase-Modulated Localized Manipulation

Besides the ability of SonoTweezer to focus US waves to trap its target agent, it can be further locally steered around the trapped position. We accomplish this steering by providing an additional phase offset to the transducers of our array that exist in the twin trap configuration, i.e., $\varphi_{\text{blue}} = 0^\circ$ and $\varphi_{\text{red}} = 180^\circ$ [defined in (4), Fig. 1(a)]. Specifically, φ_{blue} is kept fixed while φ_{red} is varied between 60° – 300° , i.e., a deviation of 120° from its mean position. We steer the trapped agent under phase modulation in two different configurations that correspond to two different directions of motion. These direction-specific configurations are denoted by $D_1(\varphi_{\text{red}})$ and $D_2(\varphi_{\text{red}})$ based on the phases in which the transducers emit φ_{red} [see Fig. 5(I)].

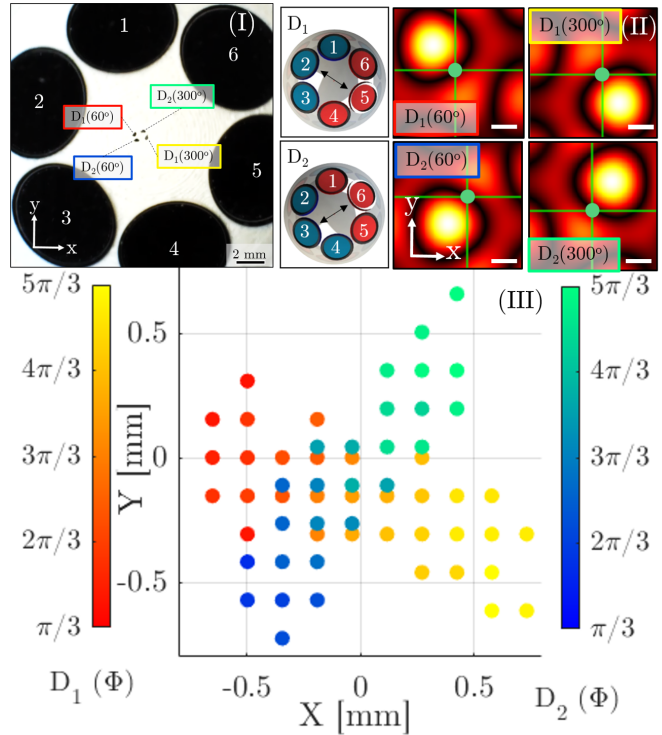


Fig. 5. Experimental results of SonoTweezer showing phase (φ) manipulation: (I) Time-lapse of a 0.5-mm polystyrene agent under two SonoTweezer φ -distributions denoted by directional configurations ($D_1(\varphi_{\text{red}})$ and $D_2(\varphi_{\text{red}})$) that are a function of $60^\circ \leq \varphi \leq 300^\circ$. D_1 denotes transducers marked 1,2,3 with blue such that $\varphi_{\text{blue}} = 0^\circ$ while D_2 denotes transducers marked 2,3,4 with blue such that $\varphi_{\text{blue}} = 0^\circ$. (II) SonoTweezer configurations D_1 and D_2 where transducers are at $\varphi_{\text{blue}} = 0^\circ$, and have a variable φ_{red} that ranges from $\varphi_{\text{red}} = 60^\circ$ – 300° . Corresponding to this φ range, the simulated pressure maps show the trapping position (green) in XY plane. Scale bar is 1 mm. (III) Extracted trapping positions of the agent over a grid of resolution 0.1 mm under $D_1(60^\circ \leq \varphi_{\text{red}} \leq 300^\circ)$ and $D_2(60^\circ \leq \varphi_{\text{red}} \leq 300^\circ)$. Please refer to the accompanying Movie S1. The trapped positions are sampled every $\varphi_{\text{red}} = 10^\circ$ interval and discretized over a grid due to the finite pixel size of the optical camera used.

In each configuration, the simulated pressure lobes that trap the agent shift from left to right in the XY plane as φ goes from 60° – 300° [see Fig. 5(II)]. Furthermore, the motion of the agent is captured under combined optical and US imaging (Movie S1). Fig. 5(III) shows the different positions of the trapped agents as it is steered along the two directions (D_1 and D_2) for constantly changing φ_{red} . Based on both simulations [see Fig. 5(II)] and experimental evidence [see Fig. 5(I) and (III)], we report that the agents can be maneuvered over a distance of 1.5 mm around its trapped position with sub-mm steps. Thus, this phase-controlled manipulation gives SonoTweezer additional freedom to perform fine spatial adjustments of its trapped agent at a target site while the array can be moved with an external manipulator.

B. Effect of Agent Size on Trapping Stability

We investigate a range of agent sizes ($d_p = 0.5$ – 2 mm) for their stable trapping and manipulation under slow movements (<5 mm/s) of SonoTweezer. These differently sized PS agents are first trapped and their stability is tested under

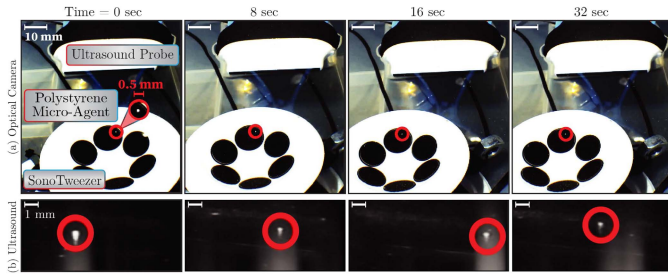


Fig. 6. Time-lapse images of a trapped 0.5-mm polystyrene agent that translates under manual movement of SonoTweezer under (a) optical camera and (b) US guidance (Please refer to accompanying Movie S3). Each image shows the trapped position of PS agent circled with red.

handheld motion of SonoTweezer. We observe that 0.5-mm agent remains stable at the trapping position and does not move from its position relative to the array as the array is moved. In contrast, the 1–1.5 mm sized agents are less stable as they constantly oscillate at their trapping position as the array moves (Please refer to accompanying Movie S2). However, the 2-mm agents are extremely unstable around their trapping position and eject out of their trap with a slight disturbance of the array. The unstable nature of larger agents (>1.5 mm) at their trapping position is due to the comparable size of the agent to that of the wavelength of sound, i.e., $\lambda \sim d_p$ [4]. Besides, the oscillatory behavior of these agents can also be attributed to nonuniform movement of SonoTweezer (1–4 mm/s), and nonspherical morphology of agents. Nonetheless, we hence infer that while SonoTweezer can reliably trap and retain 0.5-mm agents, it can also trap larger agents up to 1.5-mm agents to different degrees. Last, we demonstrate manipulation of SonoTweezer over a large square-shaped trajectory of side 30 mm with a 0.5-mm agent trapped at its focal point (see Movie S2).

C. Acoustic Manipulation Under US Imaging

Next, we demonstrate trapping and manipulation of a 0.5-mm agent under both optical camera and US imaging modality [see Fig. 6(a) and (b)]. Here, we employ the US probe at a frequency of 14 MHz in order to adequately distinguish sub-mm agents and to minimize any possible interference with the emitted waves of SonoTweezer (1 MHz). However, it is noteworthy that the pressure lobes of SonoTweezer appear as artifacts in the imaging field despite it being orthogonal to the US probe. We verified this observation with the manipulation of SonoTweezer in front of US field that confirmed these lobes to be the known cause of artifact (see Movie S3). Nevertheless, we could distinguish the agent from these artifacts based on its visibly high-intensity footprint in the imaging field. With this example, we demonstrate the combined use of US waves for both imaging and actuation of sub-mm agents which can be beneficial to clinical applications that require targeted therapy under US guidance.

D. Long-Range Manipulation With Robotic Manipulator

Finally, we interface SonoTweezer at the end-effector of a robotic manipulator (UR5) to demonstrate micromanipulation

over long trajectories (i.e., 100–150 times the agent size). First, we trap a 0.5-mm agent at the focal point of the array while it is pointing downward and immersed in water. Second, we move the end-effector of the robot (1 mm/s) along 1-D (straight line) and 2-D (L-shaped) trajectories with the trapped agent moving under camera guidance (see Movie S4). Last, we move the trapped agents over two 3-D trajectories with the robotic manipulator under the two optical cameras that enable stereo imaging of the agent [see Fig. 7(b)]. Here, we test the stability of the trap as the end-effector moves along X -, Y -, Z -directions and covers a total distance of 400 mm till the agent ejects from the trap (see Movie S4). Then, we move the end-effector along an enclosed hexagonal trajectory while the trapped agent remains trapped at the array's focal point [see Fig. 7(c)]. This enclosed trajectory is shown under both the cameras that record the end-effector time stamps [see Fig. 7(a)].

IV. CONCLUSION AND FUTURE WORK

In summary, SonoTweezer is a compact, portable, low-power, and relatively inexpensive solution to state-of-the-art waterborne phased arrays that can trap and manipulate sub-mm-sized agents. Broadly, SonoTweezer serves as an example to design customized immersible tweezers with less transducers (<10) based on the simulation and measurement approaches described in this study (see SI Appendix I). The small footprint and lightweight nature of SonoTweezer facilitates its utility as a robotic end-effector tool for contactless micromanipulation over a large distance (>100 times the size of target agent). Besides robotic end-effectors, the lightweight and portable nature of SonoTweezer could be exploited as a haptic platform to perform pick-and-place operations underwater. Alternatively, the phase-modulation over its different transducers provides sub-mm steering of the trapping position around a targeted site. This phase-modulation feature can be extended to a sophisticated actuation scheme where each of the six transducers is interfaced to three synchronized power sources such as waveform generators. As a result, phase offset combinations of all three sources can enable the trapped agent to be maneuvered over a hexagonal grid spanned by three directional configurations.

Besides the extensive phase-modulation scheme, various other considerations must be addressed in order to assess feasibility of SonoTweezer toward potential clinical applications. In particular, pressure fields of high magnitudes (~ 700 kPa–1 MPa) would be necessary to steer the trapped agents through *in vivo* tissues. Currently, as SonoTweezer is operated at pressures <300 kPa (i.e., mechanical index <0.3 [6], [18]), there is no undesirable heating or cavitation effects observed for an operation time of ~ 30 min. However, exposure to pressure magnitudes of up to ~ 1 MPa can damage the surrounding biological tissues. Thus, with the safety concerns, pulsed actuation schemes could be adopted as transducers of SonoTweezer are driven at high powers [15]. Furthermore, materials relevant to clinical applications such as cells, drugs, and microbes could be investigated for trapping in their native biological environments. Finally, a complete

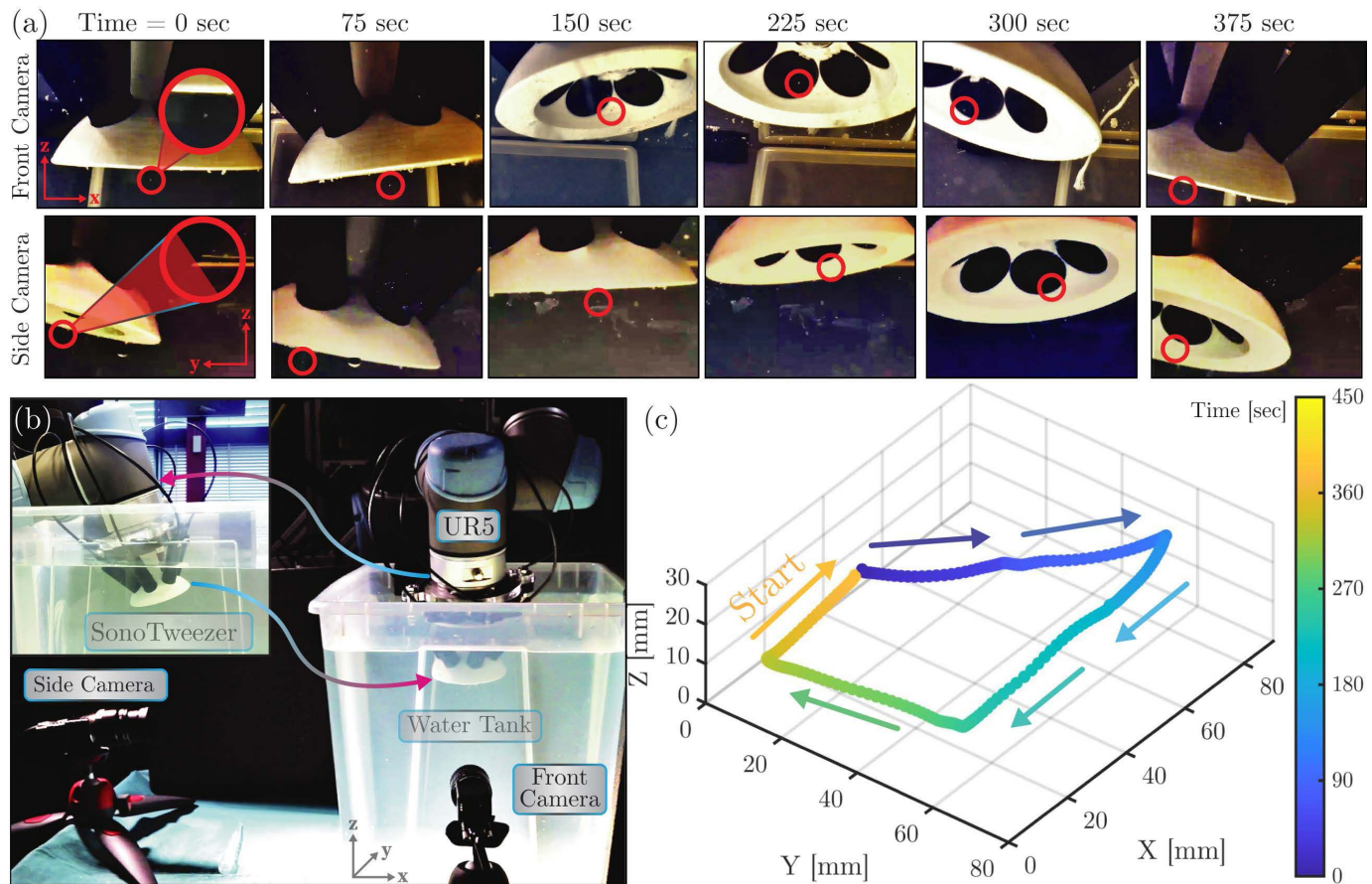


Fig. 7. (a)–(c) Demonstration of SonoTweezer as an end-effector of robotic manipulator, UR5 (Universal Robots). (b) Setup used for robotic manipulation of 0.5-mm PS agent when trapped by SonoTweezer. (a) Time-stamps of motion of robotic manipulator interfaced with SonoTweezer under two optical cameras [shown in (b)]. Each image shows the trapped position of PS agent circled with red. (c) Final trajectory of the agent under combined guidance of the two cameras with direction of arrows representing the motion of robotic manipulator. Please refer to accompanying Movie S4.

“Sono-clinical” suite may combine closed-loop control of SonoTweezer as a robotic end-effector to trap these biological agents under *ex-vivo* conditions, and to manipulate them under US guidance.

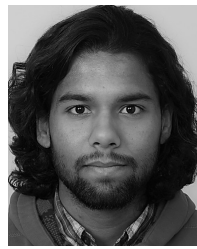
ACKNOWLEDGMENT

The authors would like to thank Dr. Arthur Berkhoff for the theoretical and experimental discussions throughout the preparation of the manuscript. They would also like to thank Dr. Olivier LeBaron (Imasonic SAS, Voray-sur-l’Ognon, France) for his scientific advice in finding the appropriate ultrasonic transducers for SonoTweezer. They would also like to thank Dr. Asier Marzo, Dr. Diego Baresch, and Dr. Milo Prsbrey for sharing their technical knowledge and experience with waterborne tweezers in course of this study.

REFERENCES

- [1] M. Sitti *et al.*, “Biomedical applications of untethered mobile milli/microrobots,” *Proc. IEEE*, vol. 103, no. 2, pp. 205–224, Feb. 2015.
- [2] Q. Wang and L. Zhang, “Ultrasound imaging and tracking of micro/nanorobots: From individual to collectives,” *IEEE Open J. Nanotechnol.*, vol. 1, pp. 6–7, 2020.
- [3] O. Erin, M. Boyvat, J. Lazovic, M. E. Tiryaki, and M. Sitti, “Wireless MRI-powered reversible orientation-locking capsule robot,” *Adv. Sci.*, vol. 8, no. 13, Jul. 2021, Art. no. 2100463.
- [4] S. Mohanty, I. S. M. Khalil, and S. Misra, “Contactless acoustic micro/nano manipulation: A paradigm for next generation applications in life sciences,” *Proc. Roy. Soc. A, Math., Phys. Eng. Sci.*, vol. 476, no. 2243, Nov. 2020, Art. no. 20200621.
- [5] B. W. Drinkwater, “A perspective on acoustical tweezers—Devices, forces, and biomedical applications,” *Appl. Phys. Lett.*, vol. 117, no. 18, Nov. 2020, Art. no. 180501.
- [6] M. A. Ghanem *et al.*, “Noninvasive acoustic manipulation of objects in a living body,” *Proc. Nat. Acad. Sci. USA*, vol. 117, no. 29, pp. 16848–16855, Jul. 2020.
- [7] M. A. B. Andrade, A. Marzo, and J. C. Adamowski, “Acoustic levitation in mid-air: Recent advances, challenges, and future perspectives,” *Appl. Phys. Lett.*, vol. 116, no. 25, Jun. 2020, Art. no. 250501.
- [8] S. A. Seah, B. W. Drinkwater, T. Carter, R. Malkin, and S. Subramanian, “Correspondence: Dexterous ultrasonic levitation of millimeter-sized objects in air,” *IEEE Trans. Ultrason., Ferroelectr., Freq. Control*, vol. 61, no. 7, pp. 1233–1236, Jul. 2014.
- [9] A. Marzo, S. A. Seah, B. W. Drinkwater, D. R. Sahoo, B. Long, and S. Subramanian, “Holographic acoustic elements for manipulation of levitated objects,” *Nat. Commun.*, vol. 6, no. 8661, pp. 1–7, 2015.
- [10] A. Marzo, A. Barnes, and B. W. Drinkwater, “TinyLev: A multi-emitter single-axis acoustic levitator,” *Rev. Sci. Instrum.*, vol. 88, no. 8, Aug. 2017, Art. no. 085105.
- [11] A. Marzo, T. Corkett, and B. W. Drinkwater, “Ultraino: An open phased-array system for narrowband airborne ultrasound transmission,” *IEEE Trans. Ultrason., Ferroelectr., Freq. Control*, vol. 65, no. 1, pp. 102–111, Jan. 2018.
- [12] G. Destgeer and H. J. Sung, “Recent advances in microfluidic actuation and micro-object manipulation via surface acoustic waves,” *Lab Chip*, vol. 15, no. 13, pp. 2722–2738, Mar. 2015.
- [13] M. Prsbrey and B. Raeymaekers, “Aligning high-aspect-ratio particles in user-specified orientations with ultrasound-directed self-assembly,” *Phys. Rev. Appl.*, vol. 12, no. 1, Jul. 2019, Art. no. 014014.

- [14] W.-C. Lo, S.-T. Kang, and C.-K. Yeh, "Transverse manipulation of microbubbles using acoustic-vortex tweezers," in *Proc. IEEE Int. Ultrason. Symp. (IUS)*, Oct. 2015, pp. 1–3.
- [15] D. Baresch and V. Garbin, "Acoustic trapping of microbubbles in complex environments and controlled payload release," *Proc. Nat. Acad. Sci. USA*, vol. 117, no. 27, pp. 15490–15496, Jul. 2020.
- [16] H. X. Cao *et al.*, "Micromotor manipulation using ultrasonic active traveling waves," *Micromachines*, vol. 12, no. 2, p. 192, Feb. 2021.
- [17] M. M. T. J. Bartels *et al.*, "Combining radiotherapy and focused ultrasound for pain palliation of cancer induced bone pain: a stage I/IIa study according to the IDEAL framework," *Clin. Transl. Radiat. Oncol.*, vol. 27, pp. 57–63, Mar. 2021.
- [18] W.-C. Lo, C.-H. Fan, Y.-J. Ho, C.-W. Lin, and C.-K. Yeh, "Tornado-inspired acoustic vortex tweezer for trapping and manipulating microbubbles," *Proc. Nat. Acad. Sci. USA*, vol. 118, no. 4, Jan. 2021, Art. no. e2023188118.
- [19] M. Azizian *et al.*, "3—The *da Vinci* surgical system," in *Handbook of Robotic and Image-Guided Surgery*. Amsterdam, The Netherlands: Elsevier, 2020, pp. 39–55, doi: [10.1016/B978-0-12-814245-5.00003-7](https://doi.org/10.1016/B978-0-12-814245-5.00003-7).
- [20] K. Khandalavala, T. Shimon, L. Flores, P. R. Armijo, and D. Oleynikov, "Emerging surgical robotic technology: A progression toward microbots," *Ann. Laparoscopic Endoscopic Surg.*, vol. 5, pp. 1–18, Nov. 2019. [Online]. Available: <https://ales.amegroups.com/article/view/5499/html>
- [21] J. Sikorski, S. Mohanty, and S. Misra, "MILiMAC: Flexible catheter with miniaturized electromagnets as a small-footprint system for micro-robotic tasks," *IEEE Robot. Autom. Lett.*, vol. 5, no. 4, pp. 5260–5267, Oct. 2020.
- [22] S. Sharma, M. Suomalainen, and V. Kyrki, "Compliant manipulation of free-floating objects," in *Proc. IEEE Int. Conf. Robot. Autom. (ICRA)*, May 2018, pp. 865–872.
- [23] C. Heunis, F. Šuligoj, C. Fambuena Santos, and S. Misra, "Real-time multi-modal sensing and feedback for catheterization in porcine tissue," *Sensors*, vol. 21, no. 1, p. 273, Jan. 2021.
- [24] S. E. Wright, A. W. Mahoney, K. M. Popek, and J. J. Abbott, "The spherical-actuator-magnet manipulator: A permanent-magnet robotic end-effector," *IEEE Trans. Robot.*, vol. 33, no. 5, pp. 1013–1024, Oct. 2017.
- [25] P. R. Slawinski, A. Z. Taddese, K. B. Musto, K. L. Obstein, and P. Valdastrì, "Autonomous retroflexion of a magnetic flexible endoscope," *IEEE Robot. Autom. Lett.*, vol. 2, no. 3, pp. 1352–1359, Jul. 2017.
- [26] C. Heunis, J. Sikorski, and S. Misra, "Flexible instruments for endovascular interventions," *IEEE Robot. Automat. Mag.*, vol. 25, no. 3, pp. 71–82, Sep. 2018.
- [27] M. Röthlisberger, M. Schuck, L. Kulmer, and J. W. Kolar, "Contactless picking of objects using an acoustic gripper," *Actuators*, vol. 10, no. 4, p. 70, Mar. 2021.
- [28] J. Nakahara, B. Yang, and J. R. Smith, "Contact-less manipulation of millimeter-scale objects via ultrasonic levitation," in *Proc. 8th IEEE RAS/EMBS Int. Conf. Biomed. Robot. Biomechatronics (BioRob)*, Nov. 2020, pp. 264–271.
- [29] A. Marzo, M. Caleap, and B. W. Drinkwater, "Acoustic virtual vortices with tunable orbital angular momentum for trapping of mie particles," *Phys. Rev. Lett.*, vol. 120, no. 4, p. 44301, Jan. 2018.
- [30] L. Gor'kov, "On the forces acting on a small particle in an acoustical field in an ideal fluid," *Sov. Phys. Doklady*, vol. 6, p. 773, Mar. 1962.
- [31] J. Bin, W. S. Oates, and K. Taira, "Thermoacoustic modeling and uncertainty analysis of two-dimensional conductive membranes," *J. Appl. Phys.*, vol. 117, no. 6, 2015, Art. no. 64506.
- [32] M. A. Ghanem, A. D. Maxwell, O. A. Sapozhnikov, V. A. Khokhlova, and M. R. Bailey, "Quantification of acoustic radiation forces on solid objects in fluid," *Phys. Rev. Appl.*, vol. 12, no. 4, Oct. 2019, Art. no. 044076.
- [33] H. Bruus, "Acoustofluidics 7: The acoustic radiation force on small particles," *Lab Chip*, vol. 12, no. 6, pp. 1014–1021, 2012.
- [34] M. Ve, "Sound reflections from concave spherical surfaces. Part II: Geometrical acoustics and engineering approach," *Acta Acustica United Acustica*, vol. 96, no. 1, pp. 92–101, 2010.
- [35] J. Li *et al.*, "Three dimensional acoustic tweezers with vortex streaming," *Commun. Phys.*, vol. 4, no. 1, p. 113, Dec. 2021.
- [36] H. Droogendijk, M. J. de Boer, R. G. P. Sanders, and G. J. M. Krijnen, "Stochastic resonance in a voltage-controlled micromechanical slider," *J. Microelectromech. Syst.*, vol. 24, no. 3, pp. 651–660, Jun. 2015.
- [37] E. A. Bunch, D. M. Altwein, L. E. Johnson, J. R. Farley, and A. A. Hammersmith, "Homogeneous sample preparation of raw shrimp using dry ice," *J. AOAC Int.*, vol. 78, no. 3, pp. 883–887, May 1995.



Sumit Mohanty received the bachelor's degree in instrumentation engineering from IIT Kharagpur, Kharagpur, India, in 2014, the master's degree in nanotechnology from the KTH Royal Institute of Technology, Stockholm, Sweden, in 2017, and the doctoral degree in biomechanical engineering from the University of Twente, Enschede, The Netherlands, in 2021.

He is currently a Post-Doctoral Fellow with the Surgical Robotics Laboratory, Department of Biomechanical Engineering, University of Twente. His research interests include design, fabrication, and actuation of magnetic and acoustic micro-robots.



Robbert-Jan Fidder received the bachelor's degree in mechanical engineering from the Windesheim University of Applied Sciences, Zwolle, The Netherlands, in 2018, and the master's degree in mechanical engineering from the University of Twente, Enschede, The Netherlands, in 2021. He was with the Surgical Robotics Laboratory, Department of Biomechanical Engineering, University of Twente, Enschede, The Netherlands, in 2021.



Pedro M. Matos is currently pursuing the integrated master's degree in bioengineering with the Faculdade de Engenharia da Universidade do Porto, Porto, Portugal. He was with the Surgical Robotics Laboratory, Department of Biomechanical Engineering, University of Twente, Enschede, The Netherlands, in 2021.



Christoff M. Heunis (Student Member, IEEE) received the M.Sc. degree in mechatronic engineering from the University of Stellenbosch, Stellenbosch, South Africa, in 2016, and the doctoral degree in surgical robotics from the University of Twente, Enschede, The Netherlands, in 2021.

He is currently a Postdoctoral Fellow with the Surgical Robotics Laboratory, University of Twente. His work focuses on adapting and integrating embedded sub-systems for health care applications, with a specific focus on surgical robotics, magnetic actuation systems, and medical image processing. His research interests include the design of clinical equipment for the treatment of endovascular, cardiovascular, and oncological disorders.



Mert Kaya (Student Member, IEEE) received the bachelor's degree in electrical and electronics engineering from Bahçeşehir University, Istanbul, Turkey, in 2011, and the master's degree in electrical and electronics engineering from Özyeğin University, Istanbul, in 2015. He is currently pursuing the doctoral degree with the Biomechanical Engineering Department, University of Twente, Enschede, The Netherlands.

He is also a Visiting Researcher with the Biomedical Engineering Department, University Medical Centre at Groningen, Groningen, The Netherlands. His research interests include surgical robotics and microrobotics.



Sarthak Misra (Senior Member, IEEE) received the master's degree in mechanical engineering from McGill University, Montreal, Canada, in 2001, and the doctoral degree in mechanical engineering from the Johns Hopkins University, Baltimore, USA, in 2009.

He is currently a Full Professor within the Department of Biomechanical Engineering, University of Twente, Enschede, The Netherlands. He is also affiliated with the Department of Biomedical Engineering, University of Groningen and University Medical Center at Groningen, The Netherlands. Prior to commencing his doctoral studies, he was a Dynamics and Controls Analyst within the International Space Station Program. His research interests include surgical robotics and medical microrobotics.

Prof. Misra was a recipient of the European Research Council Starting, Proof-of-Concept, and Consolidator Grants, and the Netherlands Organization for Scientific Research VENI and VIDI Awards. He is also the Co-Chair of the Robotics and Automation Society Technical Committee on Surgical Robotics and the International Federation of Automatic Control Technical Committee on Biological and Medical Systems.



Nathan Blanken received the bachelor's degree in applied physics from the University of Twente, Enschede, The Netherlands, in 2016, and the master's degree in physics from the University of Cambridge, Cambridge, U.K., in 2017. He is currently pursuing the doctoral degree with the Physics of Fluids Group, University of Twente, where he investigates deep learning approaches for super-resolved ultrasound imaging.

After his graduation, he was a Visiting Student with Xi'an Jiaotong University, Xi'an, China, where he studied the impact of compound drops.